

Supporting Information

A Highly Robust Cluster-Based Indium(III)-Organic Framework with Efficient Catalytic Activity on Cycloaddition of CO₂ and Knoevenagel Condensation

Hongxiao Lv, Liming Fan, Tuoping Hu, Chenxu Jiao,* and Xiutang Zhang*

School of Chemistry and Chemical Engineering, North University of China, Taiyuan 030051, People's Republic of China. E-mail: xiutangzhang@163.com.

Contents

Synthetic Procedure of H₅CPDD.

Table S1. Crystallographic data and refinement parameters of **NUC-66**.

Table S2. Selected bond lengths and angles of **NUC-66**.

Table S3. The cycloaddition reaction efficiency of various co-catalysts with **NUC-66a** and other catalysts.

Table S4. Molecular sizes of epoxides with different substituted groups.

Table S5. Comparison of the catalytic activity of various MOFs for the cycloaddition of CO₂ with epoxides.

Table S6. ICP-OES analysis of In³⁺ after 10 cycles reaction of cycloaddition and Knoevenagel Condensation.

Table S7. The Knoevenagel condensation reaction efficiency of various catalysts.

Table S8. Polarity of solvents for Knoevenagel condensation reaction.

Table S9. Molecular sizes of various benzaldehyde derivatives and products.

Table S10. Comparison of the catalytic activity of various MOFs for the Knoevenagel Condensation reaction.

Table S11. The structure details between **NUC-66** and other reported In-based MOFs

Figure S1. The PXRD patterns of as-synthesized **NUC-66** and simulated.

Figure S2. The FT-IR spectrum of as-synthesized **NUC-66** and **NUC-66a**.

Figure S3. The PXRD patterns of simulated **NUC-66** and **NUC-66a**.

Figure S4. The TGA curve of **NUC-66**.

Figure S5. The PXRD patterns of **NUC-66** sample under water treatment.

Figure S6. The N₂ absorption/desorption isotherms and pore size distribution of **NUC-66a**.

Figure S7. The CO₂ adsorption and desorption isotherms for **NUC-66a** at 273K and 298K.

Figure S8. CO₂ adsorption heat calculated by the virial equation of **NUC-66a**.

Figure S9. NH₃-TPD and CO₂-TPD profiles of **NUC-66**.

Figure S10. The GC date of 4-(hydroxymethyl)-1,3-dioxolan-2-one and 2-(phenylmethylidene)propanedinitrile.

Figure S11. The product accumulation curves with reaction time.

Figure S12. ¹H NMR spectrum of propylene carbonate.

Figure S13. ¹H NMR spectrum of 4-fluoro-1,3-dioxolan-2-one.

Figure S14. ¹H NMR spectrum of 4-chloro-1,3-dioxolane-2-one.

Figure S15. ¹H NMR spectrum of 4-ethyl-1,3-dioxolan-2-one.

Figure S16. ¹H NMR spectrum of 4-(trifluoro)-1,3-dioxolane-2-one.

Figure S17. ¹H NMR spectrum of 4-vinyl-1,3-dioxolan-2-one.

Figure S18. ¹H NMR spectrum of 4-(hydroxymethyl)-1,3-dioxolan-2-one.

Figure S19. Recyclability study for catalytic activities of **NUC-66a** in cycloaddition reaction.

Figure S20. The PXRD patterns of activated and used **NUC-66** after tenth cycloaddition reactions.

Figure S21. The FT-IR patterns of activated and used **NUC-66** after tenth cycloaddition reactions.

Figure S22. N₂ adsorption isotherms of **NUC-66a** measured after 10 cycles of cycloaddition reactions, showing negligible change in adsorption amount.

Figure S23. Evidence of heterogeneous nature of **NUC-66a** in the cycloaddition reaction.

Figure S24. ¹H NMR spectrum of 2-(phenylmethylidene)propanedinitrile.

Figure S25. ¹H NMR spectrum of 2-[(4-fluorophenyl)methylidene] propanedinitrile.

Figure S26. ¹H NMR spectrum of 2-[(4-bromophenyl)methylidene] propanedinitrile.

Figure S27. ¹H NMR spectrum of 2-[(4-nitrophenyl) methylidene] propanedinitrile.

Figure S28. ¹H NMR spectrum of 2-[(4-methylphenyl)methylidene]propanedinitrile.

Figure S29. ¹H NMR spectrum of 2-[(3,4-dimethylphenyl)methylidene]propanedinitrile

Figure S30. ^1H NMR spectrum of 2-[(3,4-dimethoxyphenyl)methylidene]propanedinitrile.

Figure S31. ^1H NMR spectrum of 2-[(3,4,5-trimethoxyphenyl)methylidene]propanedinitrile.

Figure S32. Recyclability study for catalytic activities of **NUC-66a** in Knoevenagel condensation reaction.

Figure S33. The PXRD patterns of activated and used **NUC-66** after tenth Knoevenagel condensation reactions.

Figure S34. The FT-IR patterns of activated and used **NUC-66** after tenth Knoevenagel condensation reactions.

Figure S35. N_2 adsorption isotherms of **NUC-66a** measured after Knoevenagel condensation reaction, showing negligible change in adsorption amount.

Figure S36. Evidence of heterogeneous nature of **NUC-66a** in the Knoevenagel condensation reaction.

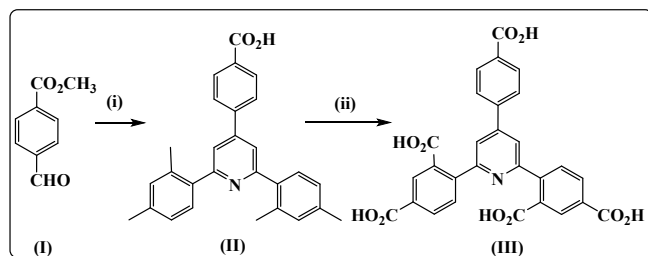
Synthetic procedure of H₅CPDD

4-(2,6-bis(2,4-dimethylphenyl)pyridin-4-yl)benzoic acid (II).

The mixture of 4-formylbenzoate (0.1 mol, 16.4 g), 2,4-dimethylacetophenone (0.2 mol, 30.0 g), and NaOH (0.31 mol, 12.2 g) was grinded into a light yellow powder, which was mixed with ammonium acetate (0.78 mol, 60.0 g) and 500 ml acetic acid. The obtained solution was refluxed for over night, cooled to ambient temperature, and further diluted by 2000 mL H₂O. The filtrated sticky crude product was recrystallized from methanol to offer the light brown sample, which was used directly for next step.

4,4'-(4-(4-carboxyphenyl)pyridine-2,6-diyl)diisophthalic acid (H₅CPDD, III).

The mixture of II (0.1 mol, 40.7 g) in mixed solvents of 500 mL pyridine and 500 mL H₂O was refluxed, and 379.2 g potassium permanganate was added step by step. After potassium permanganate was complexly added, the solution was refluxed for further 4 hs and then 100 mL ethanol was slowly added to decompose the excess of potassium permanganate. The filtrated solution was acidified to result in white product, which was recrystallized from DMF and washed with methanol. White powder was obtained with the yield of 90 %. ESI-MS: m/z [M-H]⁻, 526.09 (calcd for C₂₈H₁₇NO₁₀, 527.09). Anal. (%) calcd. for C₂₈H₁₇NO₁₀: C, 63.76; H, 3.25; N, 2.66. Found: C, 60.06; H, 3.72; N, 2.51.



Scheme S1. Synthesis precess of H₅CPDD ligand.

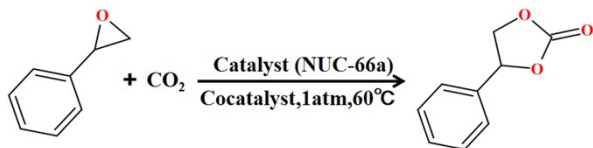
Table S1. Crystallographic data and refinement parameters of **NUC-66**.

Complex	NUC-66
Formula	C ₅₉ H ₃₀ N ₃ O ₂₆ In ₄
Mr	1654.14
Crystal system	hexagonal
Space group	P 6 ₃ /mcm
a (Å)	22.1330(2)
b (Å)	22.1330(2)
c (Å)	38.3955(3)
α (°)	90
β (°)	90
γ (°)	120
V(Å ³)	16288.8(3)
Z	6
Dcalcd(g·cm ⁻³)	1.013
μ(mm ⁻¹)	7.137
GOF	1.053
R ₁ [I > 2σ(I)]a	0.0586
wR ₂ [I > 2σ(I)]b	0.1552
R ₁ a (all data)	0.0606
wR ₂ b (all data)	0.1567
R _{int}	0.0608
^a R ₁ =Σ F _o - F _c /Σ F _o . ^b wR ₂ = Σ w(F _o ² - F _c ²) /Σ w(F _o ²) ^{1/2}	

Table S2. Selected bond lengths and angles of NUC-66.

Selected bond lengths (\AA)					
In(1)-O(1)	2.335(2)	In(1)-O(1)#1	2.335(2)	In(1)-O(6)#2	2.342(4)
In(1)-O(8)#1	2.321(4)	In(1)-O(6)#3	2.342(4)	In(1)-O(8)	2.322(4)
In(1)-O(9)	2.514(8)	In(1)-O(2)	2.342(9)	In(2)-O(1)#1	2.323(4)
In(2)-O(4)#2	2.261(4)	In(2)-O(4)#4	2.261(4)	In(2)-O(5)#5	2.196(4)
In(2)-O(5)	2.196(4)	In(2)-O(3)#6	2.404(11)	In(2)-O(3)#7	2.404(11)
In(2)-O(7)#6	2.388(11)	In(2)-O(7)#7	2.388(11)		
Selected angles ($^\circ$)					
O(1)-In(1)-O(1)#1	68.45(17)	O(1)#1-In(1)-O(6)#2	74.98(14)	O(1)#1-In(1)-O(6)#3	115.69(15)
O(1)-In(1)-O(6)#3	74.98(14)	O(1)-In(1)-O(6)#2	115.69(15)	O(1)#1-In(1)-O(9)	142.67(13)
O(1)-In(1)-O(9)	142.67(13)	O(1)-In(1)-O(2)	75.0(4)	O(1)#1-In(1)-O(2)	74.1(4)
O(6)#2-In(1)-O(6)#3	76.0(2)	O(6)#3-In(1)-O(9)	71.6(2)	O(6)#2-In(1)-O(9)	71.6(2)
O(8)#1-In(1)-O(1)#1	145.82(17)	O(8)-In(1)-O(1)#1	91.32(16)	O(8)#1-In(1)-O(1)	91.32(16)
O(8)-In(1)-O(1)	145.82(17)	O(8)#1-In(1)-O(6)#2	139.11(17)	O(8)#1-In(1)-O(6)#3	82.85(17)
O(8)-In(1)-O(6)#3	139.11(17)	O(8)-In(1)-O(6)#2	82.84(17)	O(8)#1-In(1)-O(8)	91.3(3)
O(8)-In(1)-O(9)	68.6(2)	O(8)#1-In(1)-O(9)	68.6(2)	O(8)#1-In(1)-O(2)	74.1(5)
O(8)-In(1)-O(2)	73.0(4)	O(2)-In(1)-O(6)#3	141.4(6)	O(2)-In(1)-O(6)#2	139.9(6)
O(2)-In(1)-O(9)	124.7(3)	O(1)#1-In(2)-O(3)#4	152.6(3)	O(1)#1-In(2)-O(3)#5	152.6(3)
O(1)#1-In(2)-O(7)#4	152.7(3)	O(1)#1-In(2)-O(7)#5	152.7(3)	O(4)#2-In(2)-O(1)#1	79.75(12)
O(4)#6-In(2)-O(1)#1	79.75(12)	O(4)#6-In(2)-O(4)#2	84.1(2)	O(4)#2-In(2)-O(3)#5	107.2(5)
O(4)#2-In(2)-O(3)#4	74.9(4)	O(4)#6-In(2)-O(3)#4	107.2(5)	O(4)#2-In(2)-O(7)#4	122.8(5)
O(4)#6-In(2)-O(3)#5	74.9(4)	O(4)#6-In(2)-O(7)#4	87.0(4)	O(4)#2-In(2)-O(7)#5	87.0(4)
O(4)#6-In(2)-O(7)#5	122.8(5)	O(5)-In(2)-O(1)#1	82.94(16)	O(5)#7-In(2)-O(1)#1	82.94(16)
O(5)#7-In(2)-O(4)#6	89.88(19)	O(5)-In(2)-O(4)#2	89.88(19)	O(5)-In(2)-O(4)#6	162.43(17)
O(5)#7-In(2)-O(4)#2	162.43(17)	O(5)-In(2)-O(5)#7	91.0(3)	O(5)-In(2)-O(3)#5	122.7(4)
O(5)#7-In(2)-O(3)#4	122.7(4)	O(5)#7-In(2)-O(3)#5	87.0(4)	O(5)-In(2)-O(3)#4	87.0(4)
O(5)-In(2)-O(7)#5	73.2(4)	O(5)#7-In(2)-O(7)#4	73.2(4)	O(5)#7-In(2)-O(7)#5	110.0(5)
O(5)-In(2)-O(7)#4	110.0(5)	O(3)#4-In(2)-O(3)#5	49.2(5)	O(7)#4-In(2)-O(3)#5	18.2(3)
Symmetry transformations used to generate equivalent atoms: $^1x,y,-z+3/2$; $^2y-x,-x+1,z$; $^3y-x,-x+1,-z+3/2$; $^4x-y+1,x,-z+1$; $^5x,x-y+1,-z+1$; $^6-x+1,y-x,-z$; 7y,x,z ; $^8y,x,-z+3/2$; $^9-y+1,x-y+1,z$; $^{10}x-y+1,-y+2,z$; $^{11}y,y-x+1,-z+1$;					

Table S3. The cycloaddition reaction efficiency of various co-catalysts with **NUC-66a** and other catalysts.^a



Entry	Catalyst (mol%)	Cocatalyst (mol%)	Temp. (°C)	Time (h)	Sel. (%) ^b	Yield (%) ^c	TOF (h ⁻¹) ^d
1	NUC-66a	KCl	60	8	64	2	2
2	NUC-66a	KI	60	8	73	3	3
3	NUC-66a	KBr	60	8	85	5	5
4	NUC-66a	<i>n</i> -Pr ₄ NBr	60	8	80	29	29
5	NUC-66a	<i>n</i> -Et ₄ NBr	60	8	85	33	33
6	NUC-66a	<i>n</i> -Me ₄ NBr	60	8	90	25	25
7	NUC-66a	<i>n</i> -Bu ₄ NBr	60	8	99	95	95
8	NUC-66a	<i>n</i> -Bu ₄ NI	60	8	92	75	75
9	NUC-66a	<i>n</i> -Bu ₄ NCl	60	8	90	80	80
10	NUC-66	<i>n</i> -Bu ₄ NBr	60	8	86	38	38
11	NUC-66a	-	60	8	80	11	11
12	-	<i>n</i> -Bu ₄ NBr	60	8	81	19	-
13	In ₂ O ₃	-	60	8	51	8	8
14	In(NO ₃) ₃	-	60	8	49	6	6
15	In ₂ O ₃	<i>n</i> -Bu ₄ NBr	60	8	83	42	42
16	In(NO ₃) ₃	<i>n</i> -Bu ₄ NBr	60	8	79	36	36

^aReaction conditions: Substrates (20 mmol), **NUC-66a** catalyst (0.5 mol %), Cocatalyst (4.0 mol %), CO₂ (1 atm);

^bSel.(%) = amount of targeted product/amount of converted raw materials. ^cChecked by GC. ^dTOF =turnover number (defined as moles of the product/mole of the catalyst)/reaction time.

Table S4. Molecular sizes of epoxides and products with different substituted groups.

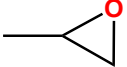
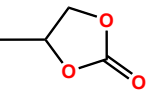
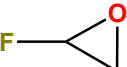
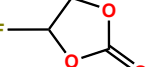
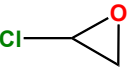
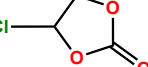
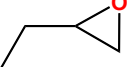
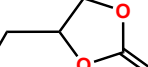
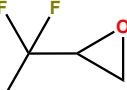
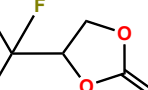
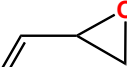
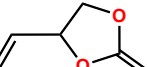
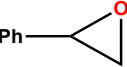
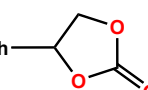
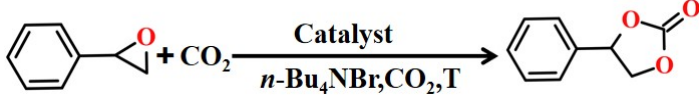
Entry	Epoxides	Molecular Size (Å ³)	Products	Molecular Size (Å ³)
1		4.9×4.4×4.6		5.7×4.4×4.8
2		4.4×3.7×4.3		5.5×4.2×4.3
3		4.6×3.8×4.4		5.9×4.4×4.6
4		5.2×3.8×4.5		6.5×4.6×4.8
5		5.5×4.5×3.9		6.3×3.1×4.4
6		5.7×4.5×4.9		6.4×4.3×4.9
7		6.0×4.4×6.8		7.8×4.1×5.3

Table S5. Comparison of the catalytic activity of various MOFs for the cycloaddition of CO₂ with epoxides.

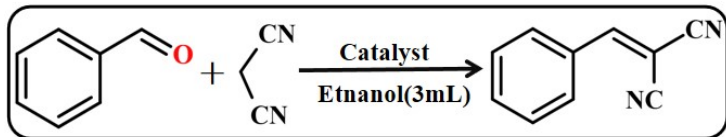


MOF	Catalyst (mmol)	n-Bu ₄ NBr (mmol)	Temp. (°C)	Pressure (atm)	Time (h)	Yield (%)	TOF (h ⁻¹)	Ref.
1	0.5	1.0	40	1	20	83	8.3	S1
Zn-2PDC	0.5	3.6	rt	10	12	98	16.7	S2
UiO-66-Gua0.2(s)	0.6	0.8	70	1	12	96	13	S3
1a	0.4	0.5	60	1	12	97	20.2	S4
1	0.5	5	60	2	6	65	22	S5
MOF	0.8	0.7	85	5	5	92.6	23.1	S6
Zn_{0.75}Mg_{0.25}-MOF-74	0.59	0.9	60	8	5	99	33	S7
Cd₆(TPOM)₃(L)₆	0.5	1.0	40	1	20	99	10	S8
ADES-3	2.0	2.5	80	10	8	99	155	S9
NUC-66	0.5	4.0	60	1	8	95	95	Our

Table S6. ICP-OES analysis of In³⁺ after 10 cycles reaction of cycloaddition reaction^a and Knoevenagel condensation reaction^b.

Catalyst	In ³⁺ concentration (%) ^a	In ³⁺ concentration (%) ^b
NUC-66a	0.0276	0.0302

Table S7. The Knoevenagel condensation reaction efficiency of various catalysts.^a



Entry	Catalyst (mol%)	Sel. (%) ^c	Yield (%) ^d
1 ^b	NUC-66	88	35
2	In ₂ O ₃	56	10
3	In(NO ₃) ₃	47	7

^aReaction conditions: Catalyst (0.5 mol %), malononitrile (20 mmol), aldehyde derivatives (10 mmol), ethanol 3mL, 6 h, 55 °C. ^bNUC-66: original sample without treatment. ^cSel.(%) = amount of targeted product/amount of converted raw materials. ^dChecked by GC.

Table S8. Polarity of solvents for Knoevenagel condensation reaction.

Entry	Solvent	Polarity (SPP) ^{S10,S11}
1	EtOH	0.85
2	DMF	0.95
3	MeOH	0.86
4	THF	0.84
5	Toluene	0.66
6	Cyclohexane	0.56

Table S9. Molecular sizes of various benzaldehyde derivatives and products.

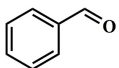
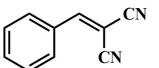
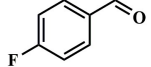
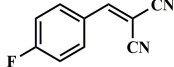
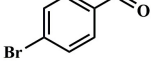
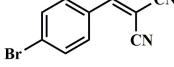
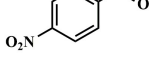
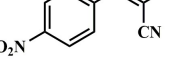
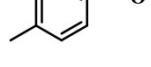
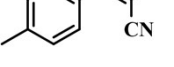
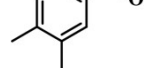
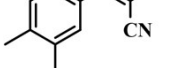
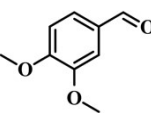
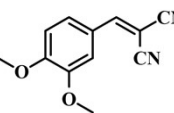
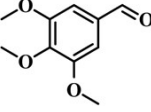
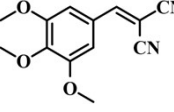
Entry	Substrates	Molecular Size (Å ³)	Products	Molecular Size (Å ³)
1		8.6×7.2×2.4		9.3×7.7×3.0
2		9.1×7.0×2.9		9.8×7.5×3.2
3		9.9×6.8×2.5		10.4×7.5×3.2
4		9.8×7.1×4.2		10.5×7.7×5.0
5		9.5×7.0×4.2		10.8×7.8×5.0
6		10.5×8.4×7.1		11.0×9.0×8.8
7		11.0×8.8×7.9		11.4×9.2×8.5
8		11.6×9.0×8.1		12.0×9.8×9.0

Table S10. Comparison of the catalytic activity of various MOFs for the Knoevenagel Condensation reaction.

MOF	Catalyst (mol %)	Solvent	Temp. (°C)	Time (h)	Yield (%)	TOF (h⁻¹)	Ref.
Tb-DCBA	10 wt%	CH ₂ Cl ₂	RT	6	99	-	S12
JLU-MOF112	0.25	EtOH	60	2	98	196	S13
1	2.0	MeOH	27	1		50	S14
[Tm ₃ (BDCP) ₂ (H ₂ O) ₃	0.4	EtOH	80	24	99	10.3	S15
[Y ₃ (μ ₃ -O) ₂ (μ ₃ -OH)(H ₂ O) ₂ (BTCTBA) ₂	0.25	EtOH	60	3	98	130.6	S16
1·Cd	0.6	-	60	1	95	158.4	S17
1	0.3	-	60	1	99	167	S18
[Co ₂ (bptc)(H ₂ O) ₂] · 5DMA	2	-	60	6	99	8.3	S19
Yb ₄ (BDCP) ₂ (μ ₃ -OH) ₂ (μ ₂ -HCO ₂)(H ₂ O) ₂	0.3	EtOH	45	24	96	53	S20
NUC-66a	0.5	EtOH	55	6	97	129	Our

Table S11. The structure details between NUC-66 and other reported In-based MOFs.

Complex	Ligand	SBU	Nuclear count	Crystal system	Ref.
NUC-66	H ₅ CPDD	[In ₄ (μ ₃ -OH) ₂ (COO) ₁₀ (DMF)(H ₂ O) ₂]	Four	Hexagonal	Our
2	2,6-H ₂ pydc/1,4-H ₂ bda	{In ₄ (μ ₂ -OH) ₃ }	Four	Rhombohedral	S21
In-PMOF	TCPP	-	-	Monoclinic	S22
ZJNU-121	H ₄ L	In ₂ (OH) ₂ (COO) ₂	Multinuclear	Orthorhombic	S23
In-TATAB	H ₃ TATAB	[In ₃ O(TATAB) ₂ (H ₂ O) ₃]	Three	Tetragonal	S24
NU-50	H ₄ TBAPy	In(COO) ₄ ⁻	One	Orthorhombic	S25
UPC-100-In	H ₄ DCBA	In(RCOO) ₄	One	Monoclinic	S26

Molecular formulas:

NUC-66: {[In₄(CPDD)₂(μ₃-OH)₂(DMF)(H₂O)₂]·2DMF·5H₂O}_n

2: {[In_{4/3}(μ₂-OH)(2,6-pydc)(1,4-bda)_{0.5}(H₂O)]·2H₂O}_n

In-PMOF: C₅₂H₄₀InN₆O₈Pd

ZJNU-121: In₂(OH)₂(L)

In-TATAB: [In₃O(TATAB)₂(H₂O)₃](NO₃)·(DMA)₁₅

NU-50: InC₄₆H₃₀NO₈

UPC-100-In: {[In(DCBA)(MeNH₃)] · DMF · 3H₂O}

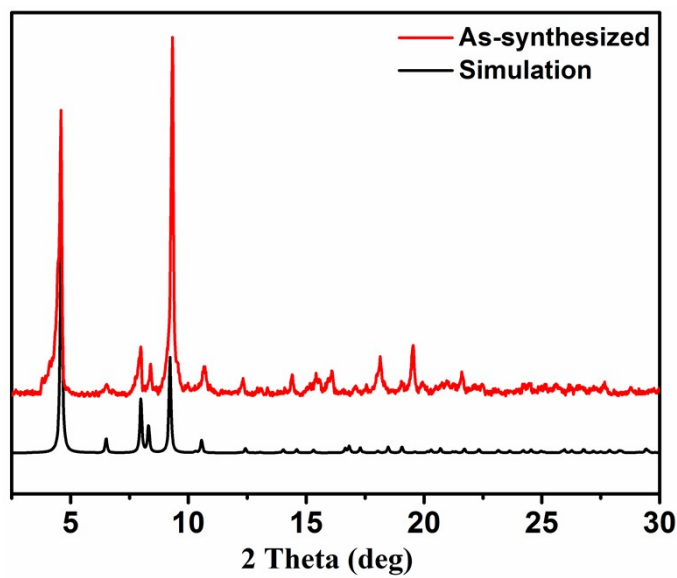


Figure S1. The PXRD patterns of as-synthesized NUC-66 and simulated one.

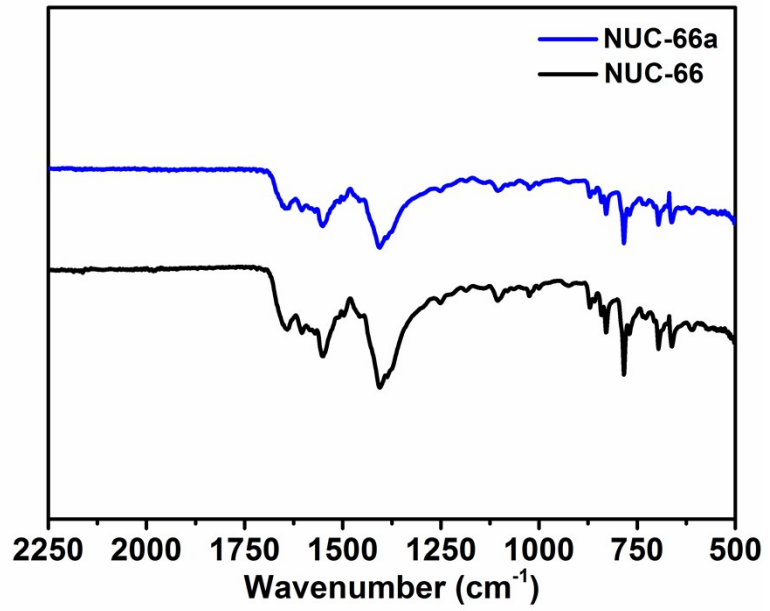


Figure S2. The FT-IR spectrum of as-synthesized **NUC-66** and activated **NUC-66a**.

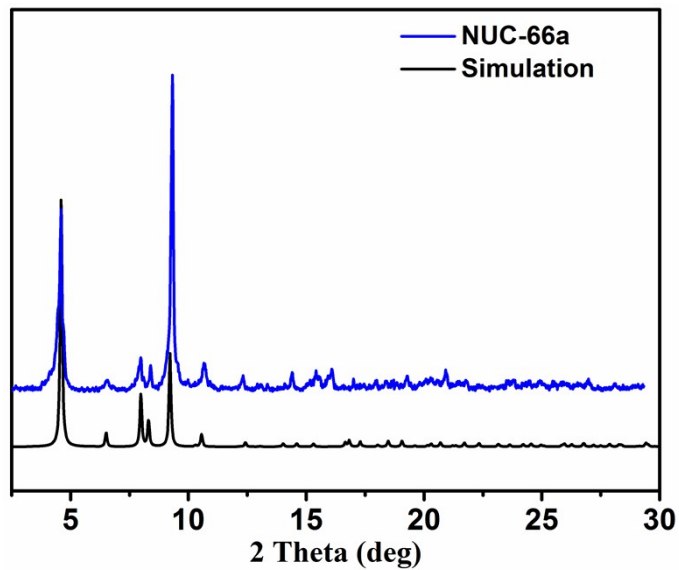


Figure S3. The PXRD patterns of simulated **NUC-66** and **NUC-66a**.

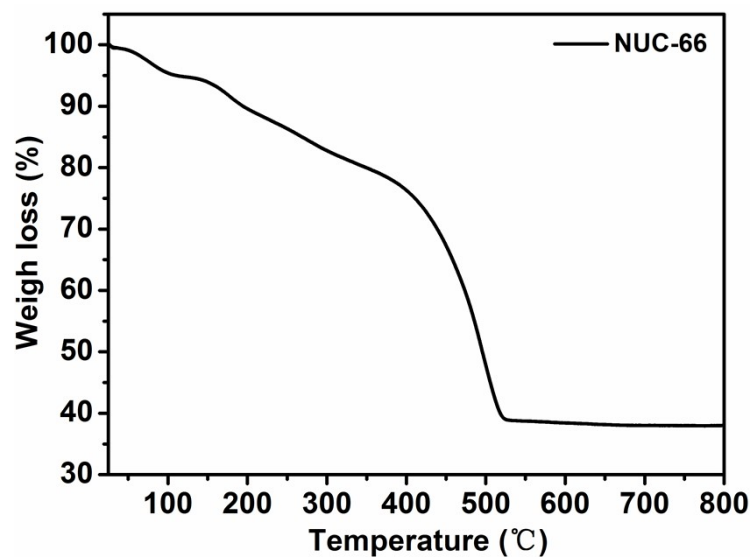


Figure S4. The TGA curve of NUC-66.

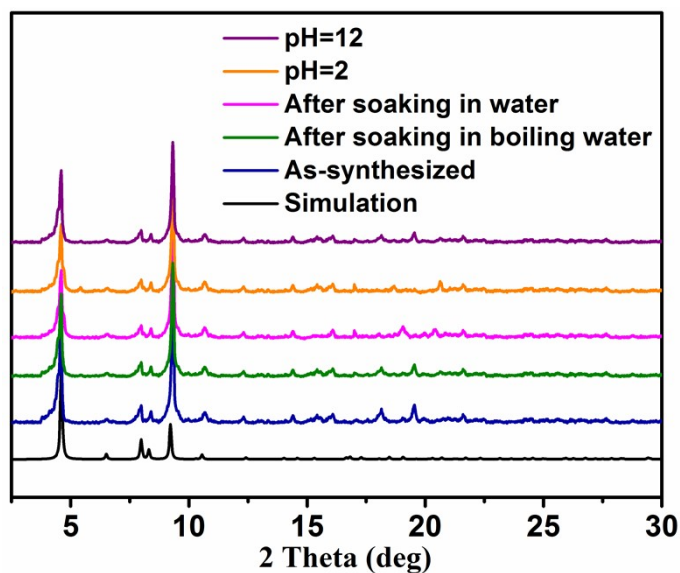


Figure S5. The PXRD patterns of NUC-66 sample under water treatment.

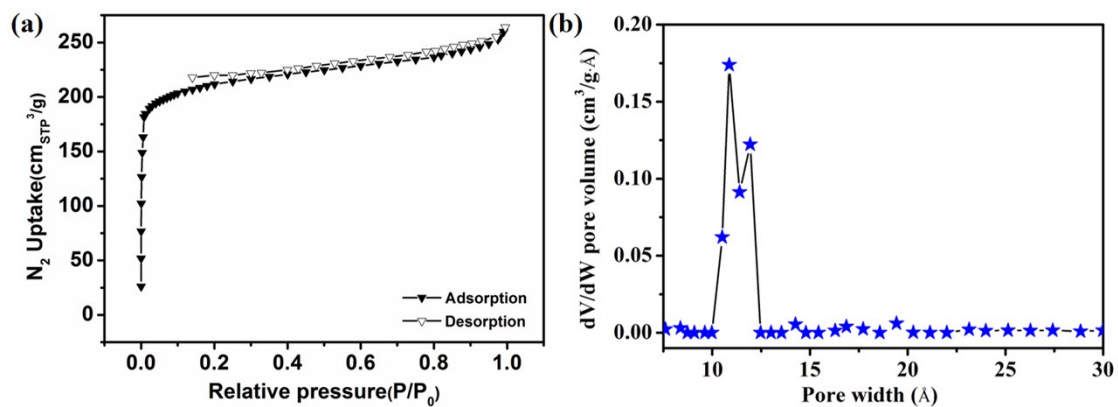


Figure S6. The N₂ absorption/desorption isotherms and pore size distribution of NUC-66a.

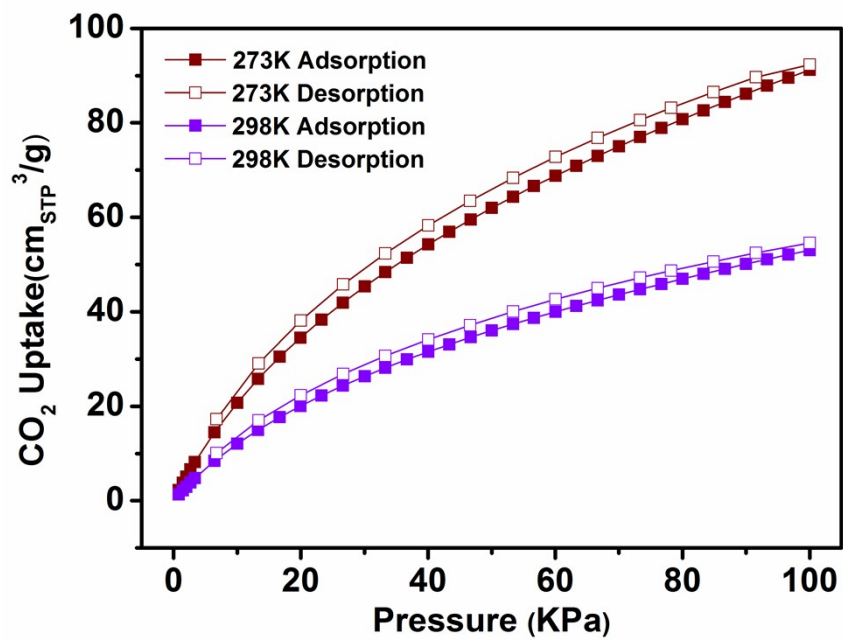


Figure S7. The CO₂ adsorption and desorption isotherms for NUC-66a at 273K and 298K.

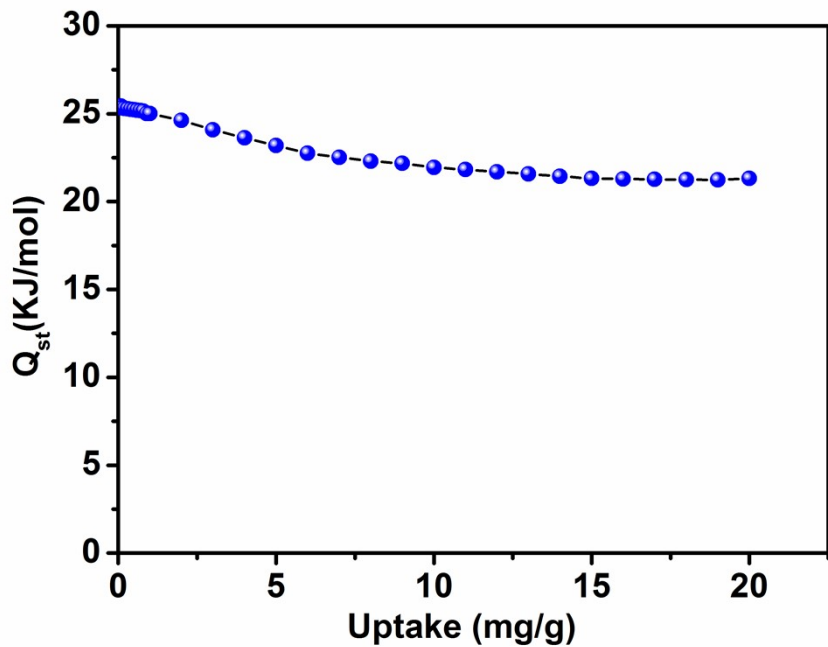


Figure S8. CO₂ adsorption heat calculated by the virial equation of **NUC-66a**.

Isosteric Heat Calculation.

The Q_{st} value is a parameter that describes the average enthalpy of adsorption for an adsorbing gas molecule at a specific surface coverage and is usually evaluated using two or more adsorption isotherms collected at similar temperatures. The zero-coverage isosteric heat of adsorption is evaluated by first fitting the temperature-dependent isotherm data to a virial-type expression, which can be written as:

$$\ln p = \ln N + \frac{1}{T} \sum_{i=0}^m a_i N^i + \sum_{j=0}^n b_j N^j$$

N: Adsorption capacity (mg/g); p: Pressure (mmHg); T: Temperature (K); a_i , b_j : Empirical constant; R : Universal gas constant (8.314 J·mol⁻¹·K⁻¹)

The isosteric enthalpy of adsorption (Q_{st}) :

$$Q_{st} = -R \sum_{i=0}^m a_i N^i$$

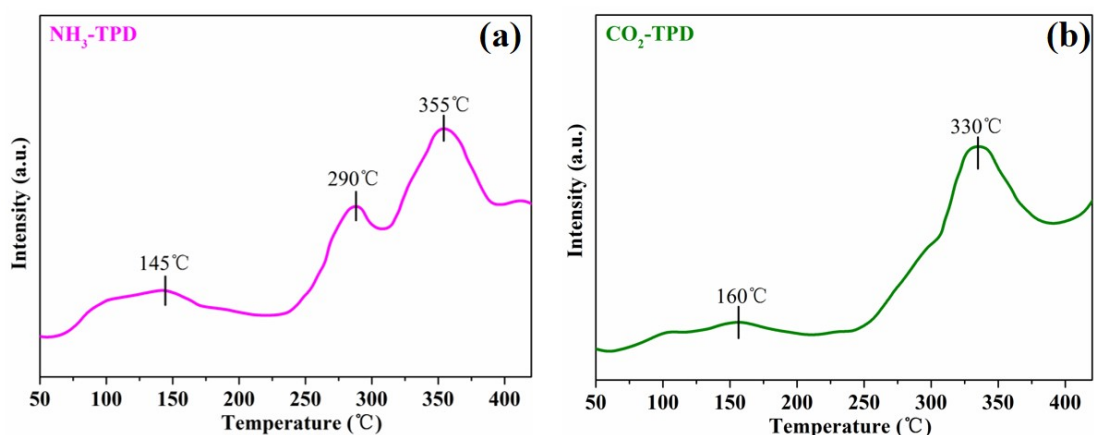


Figure S9. NH₃-TPD and CO₂-TPD profiles of NUC-66.

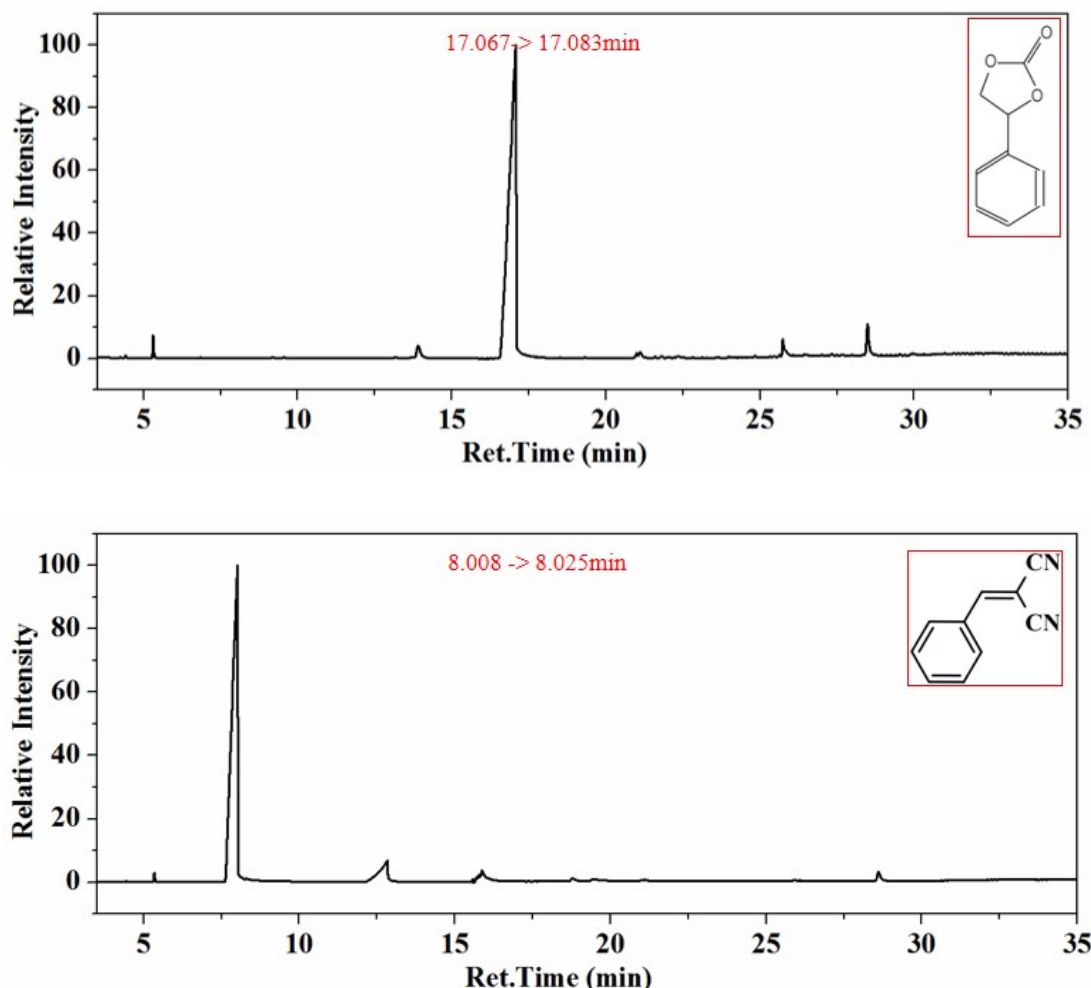


Figure S10. The GC date of 4-(hydroxymethyl)-1,3-dioxolan-2-one and 2-(phenylmethylidene)propanedinitrile.

Yield Calculation Based on the GC Analysis

Gas chromatography analyses were executed on a gas chromatography instrument (Shimadzu, GC-2014C with a PC-624 (V) capillary column and FID detector), the yield (%) was calculated based on the consumption of starting material using the equation:

$$\text{Yield (\%)} = \left(\frac{\frac{\text{area of reactant at 0 hour}}{\text{area of interal standard at 0 hour}} - \frac{\text{area of reactant at any time}}{\text{area of interal standard at any time}}}{\frac{\text{area of reactant at 0 hour}}{\text{area of interal standard at 0 hour}}} \right)$$

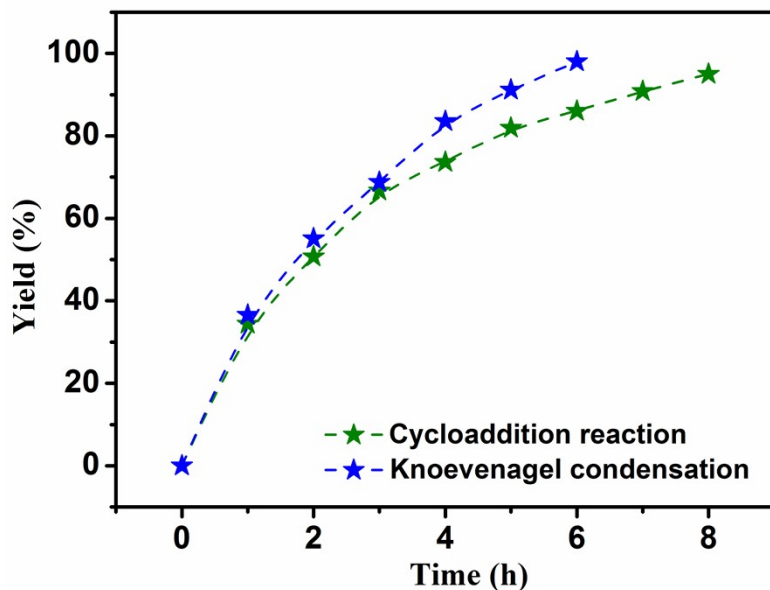


Figure S11. The product accumulation curves with reaction time.

The kinetic studies demonstrate that the multiple of TOF value difference obtained from yields and reaction rates is about 50% to 300%, whose value belongs to the same order.

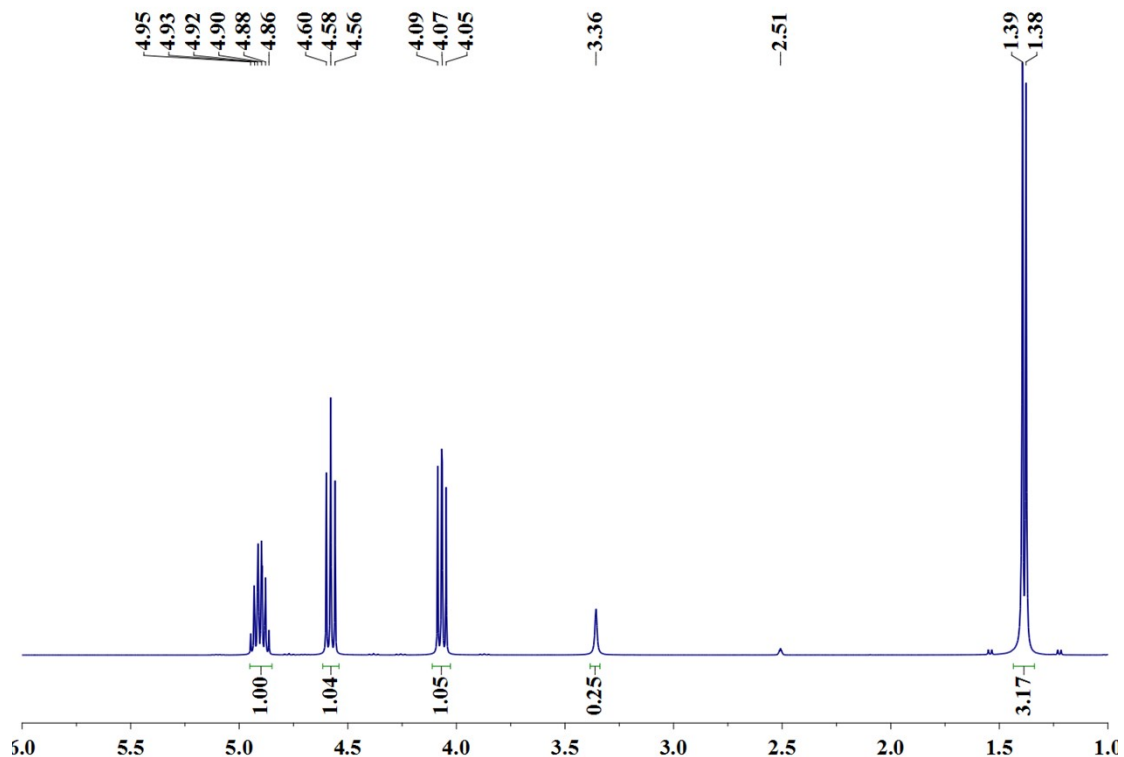


Figure S12. ¹H NMR spectrum of propylene carbonate.

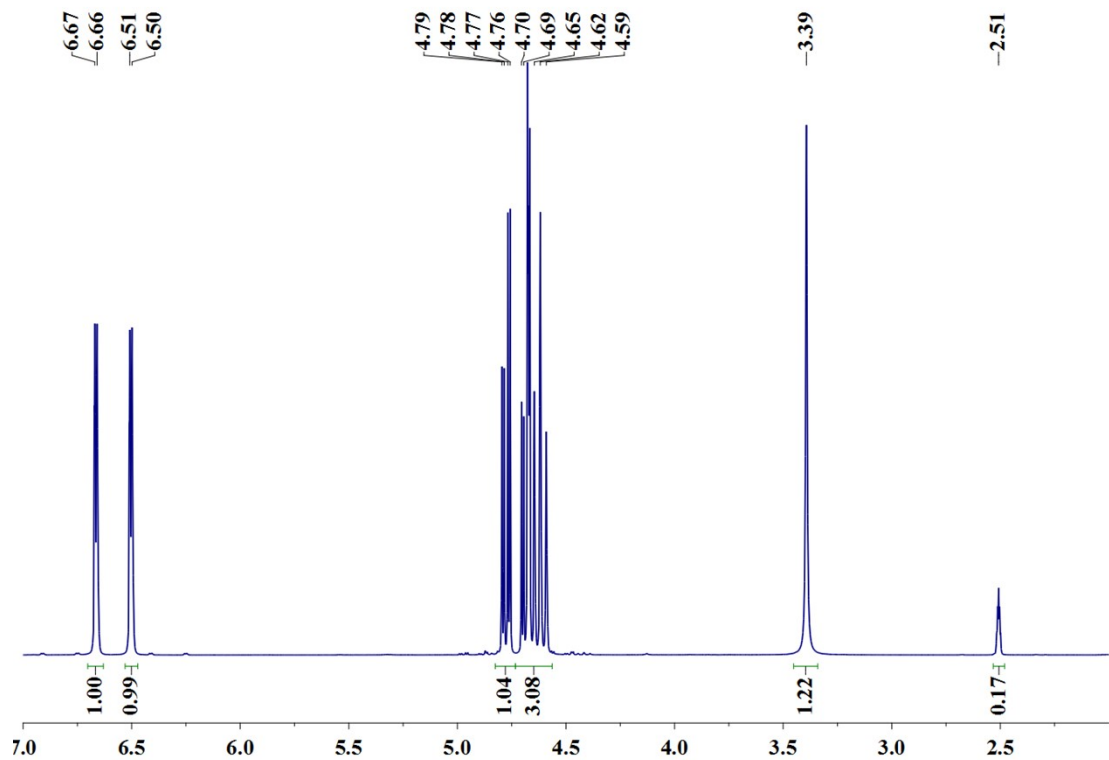


Figure S13. ¹H NMR spectrum of 4-fluoro-1,3-dioxolan-2-one.

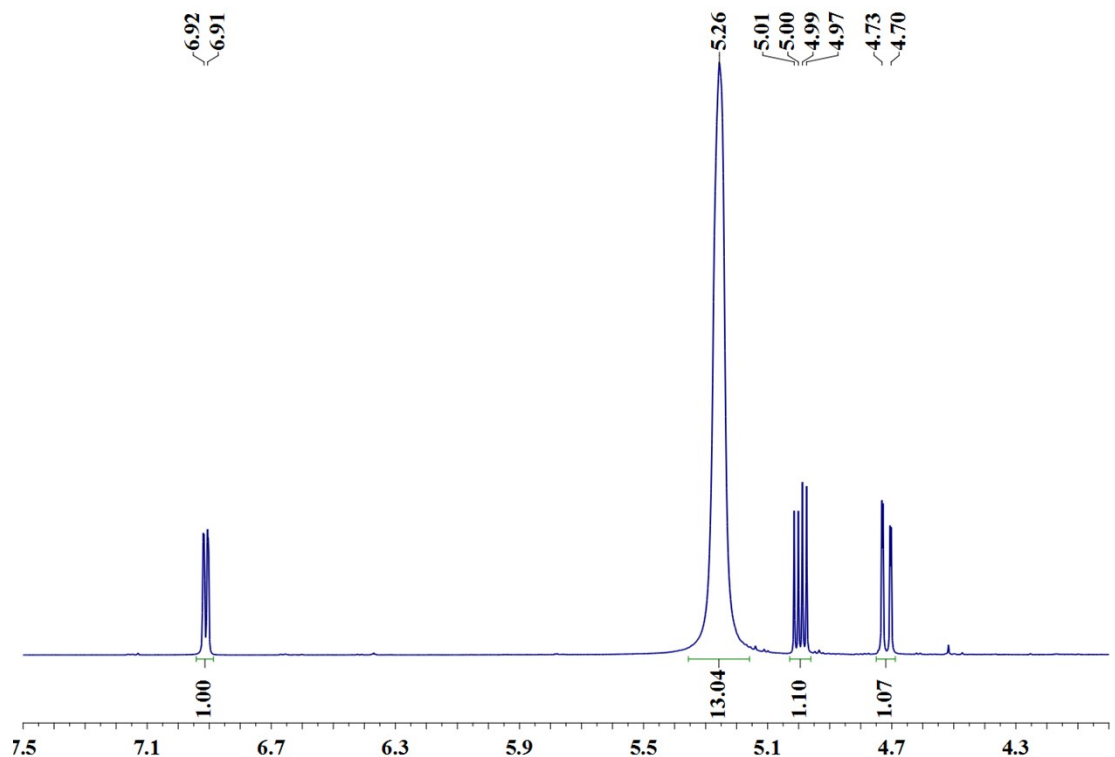


Figure S14. ${}^1\text{H}$ NMR spectrum of 4-chlorine-1,3-pentamine-2-ketone.

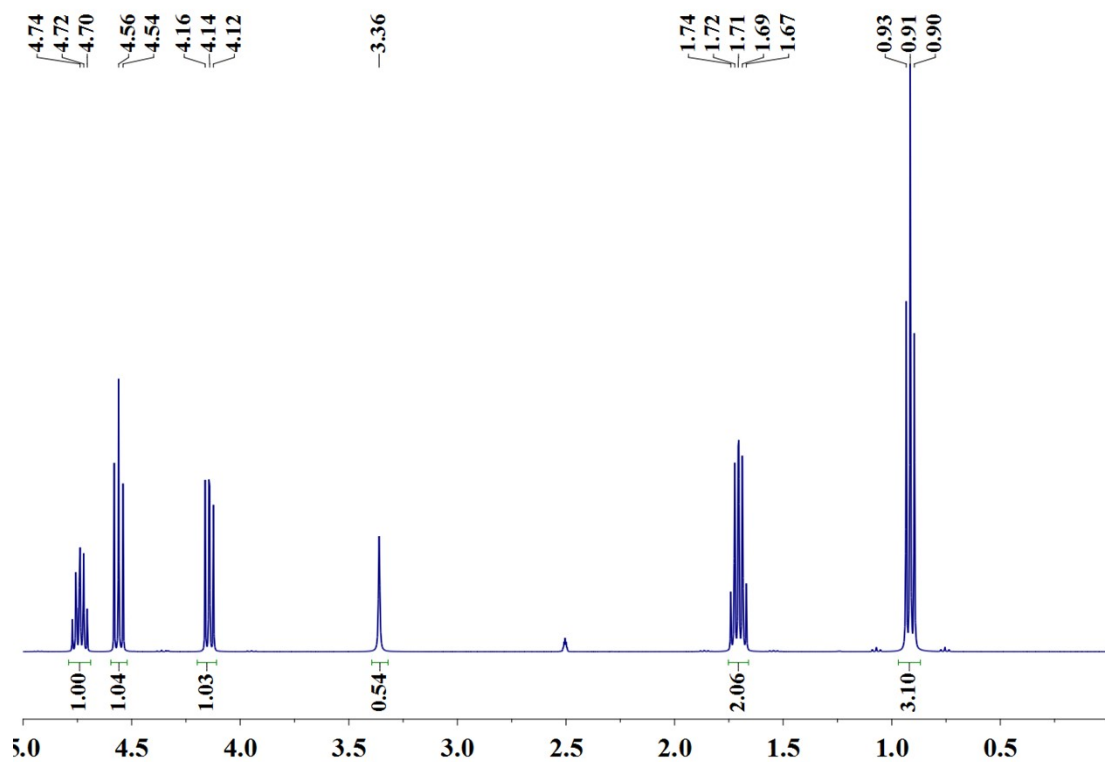


Figure S15. ^1H NMR spectrum of 2-(trifluoromethyl)oxirane.

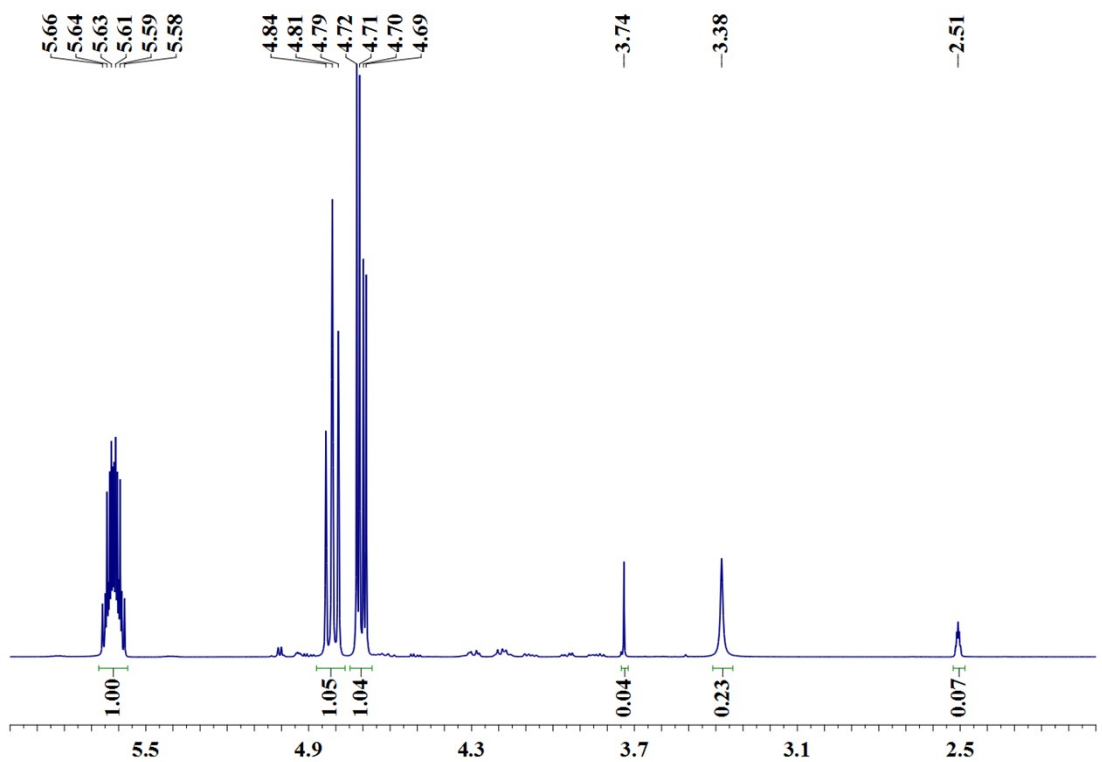


Figure S16. ¹H NMR spectrum of 1,2-butylene carbonate.

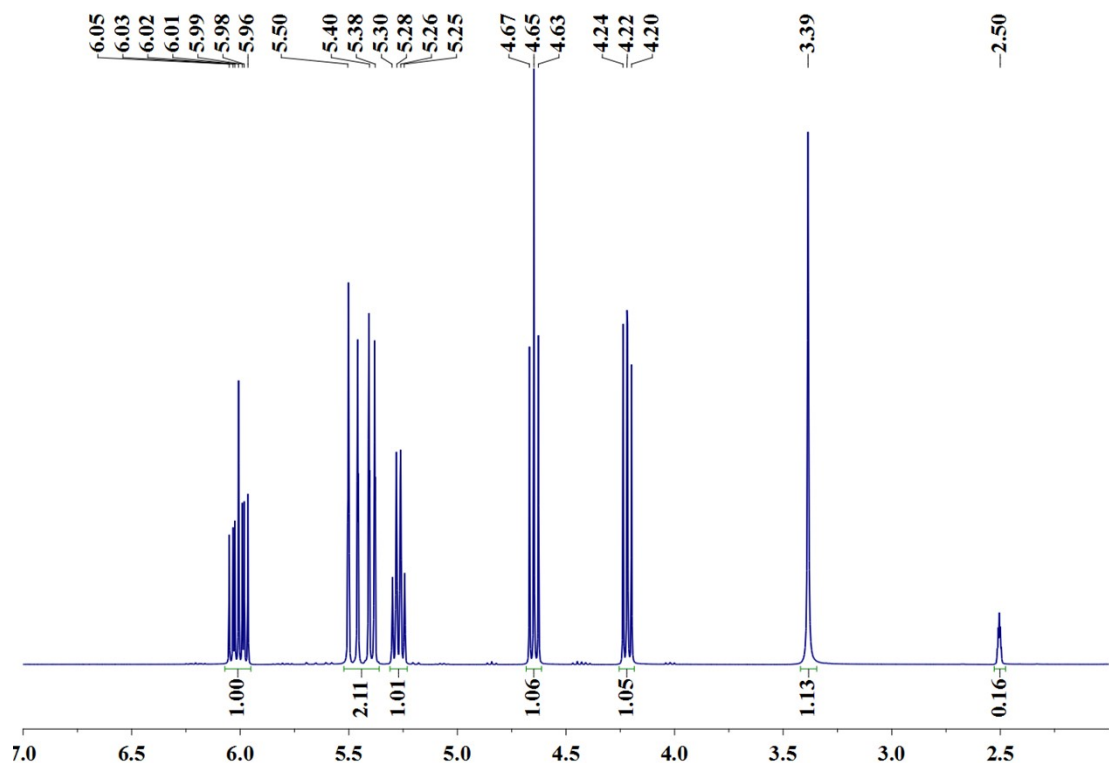


Figure S17. ^1H NMR spectrum of 4-vinyl-1,3-dioxolan-2-one.

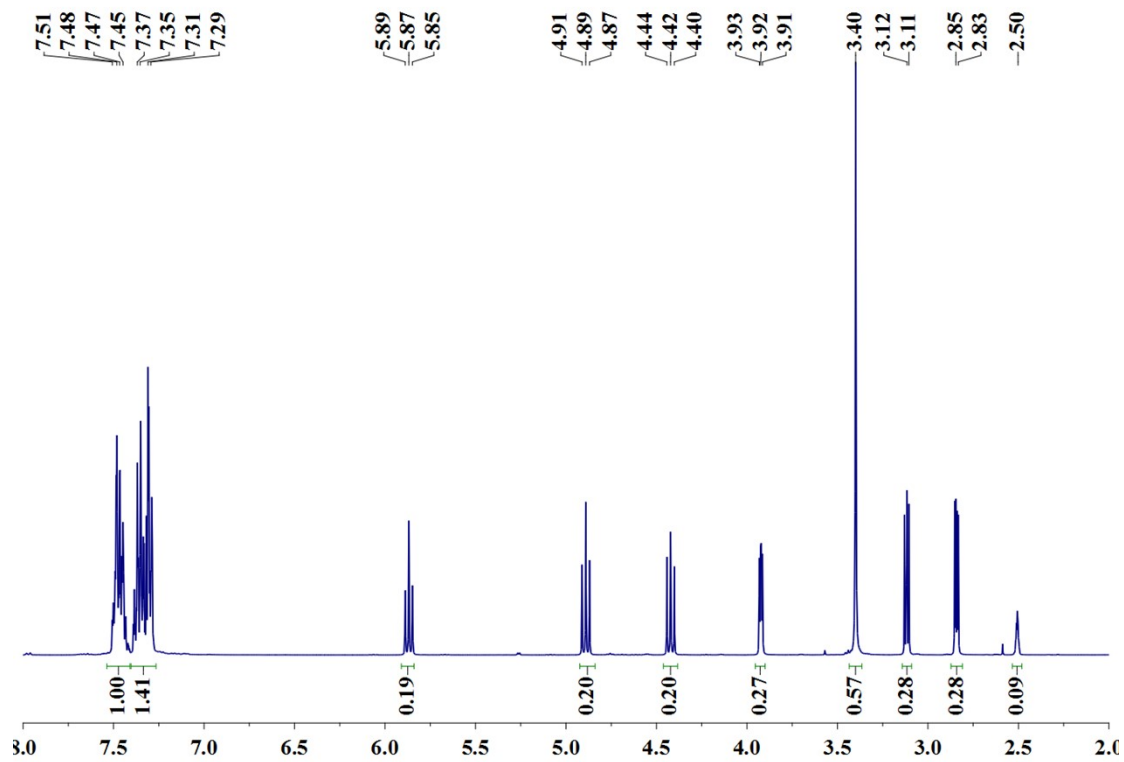


Figure S18. ^1H NMR spectrum of 4-(hydroxymethyl)-1,3-dioxolan-2-one.

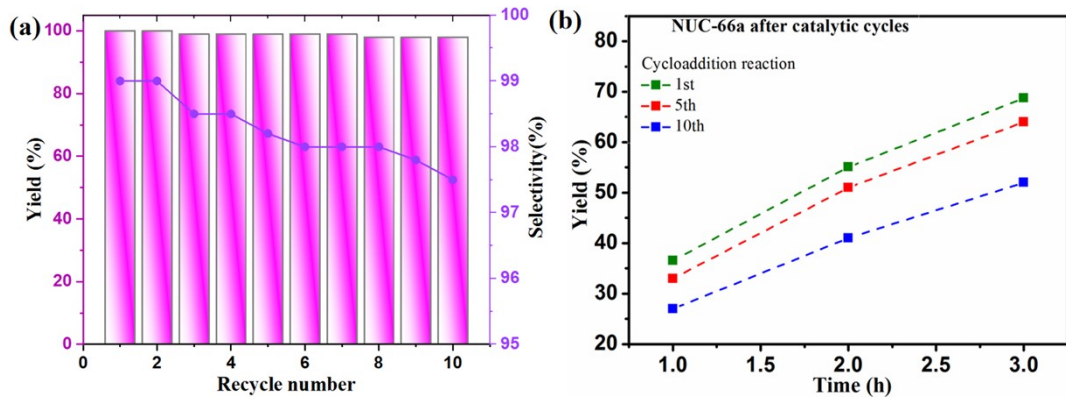


Figure S19. Recyclability study for catalytic activities of NUC-66a in cycloaddition reaction.

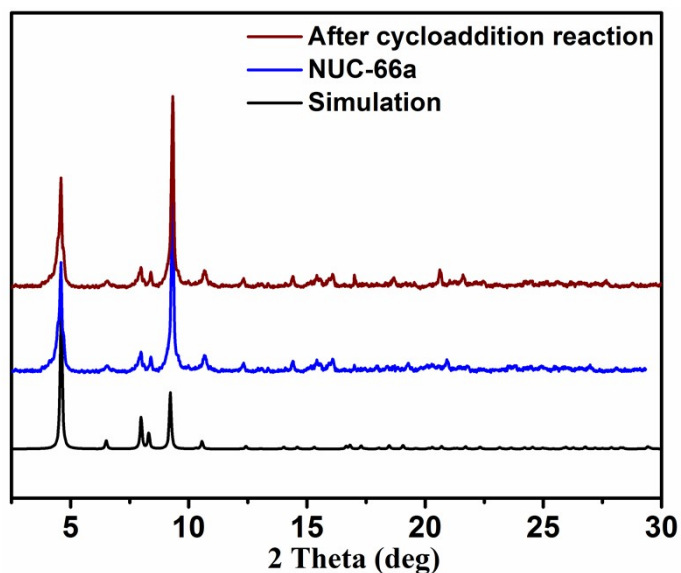


Figure S20. The PXRD patterns of activated and used **NUC-66** after tenth cycloaddition reactions.

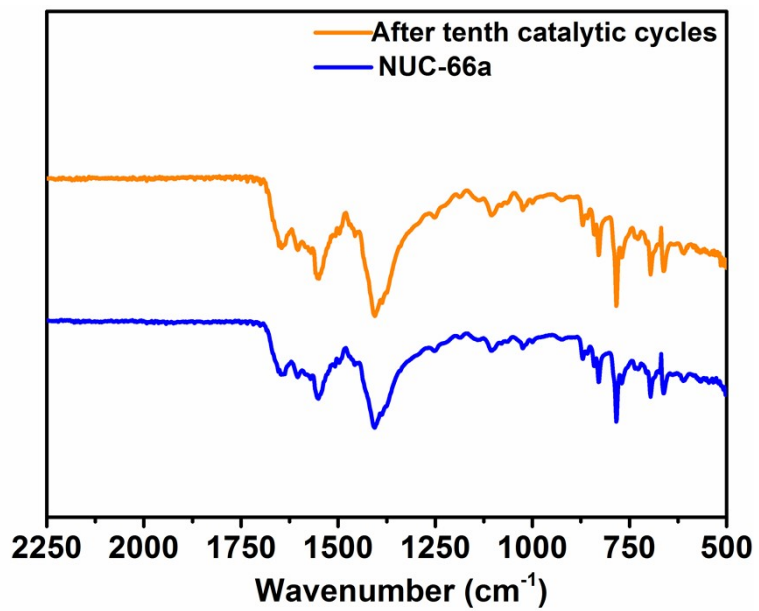


Figure S21. The FT-IR patterns of activated and used **NUC-66** after tenth cycloaddition reactions.

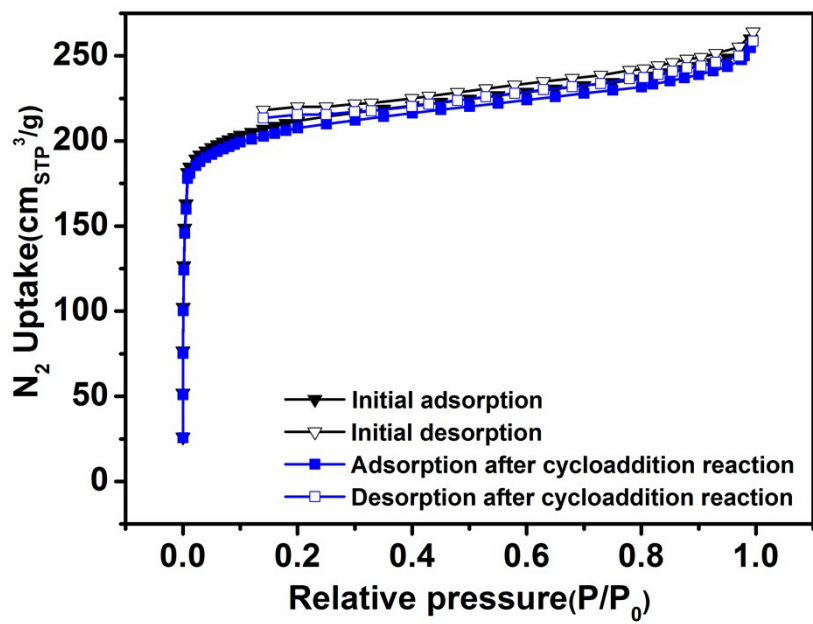


Figure S22. N₂ adsorption isotherms of **NUC-66a** measured after 10 cycles of cycloaddition reactions, showing negligible change in adsorption amount.

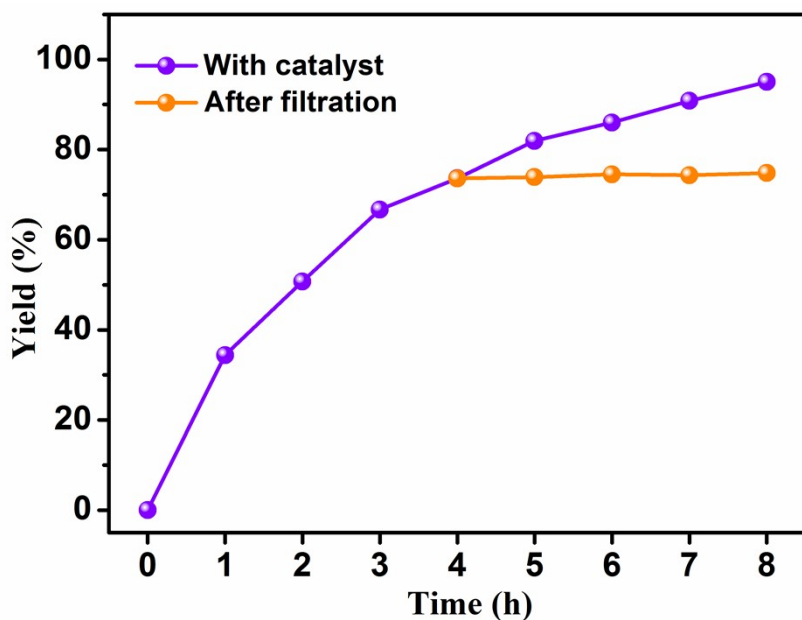


Figure S23. Evidence of heterogeneous nature of NUC-66a in the cycloaddition reaction.

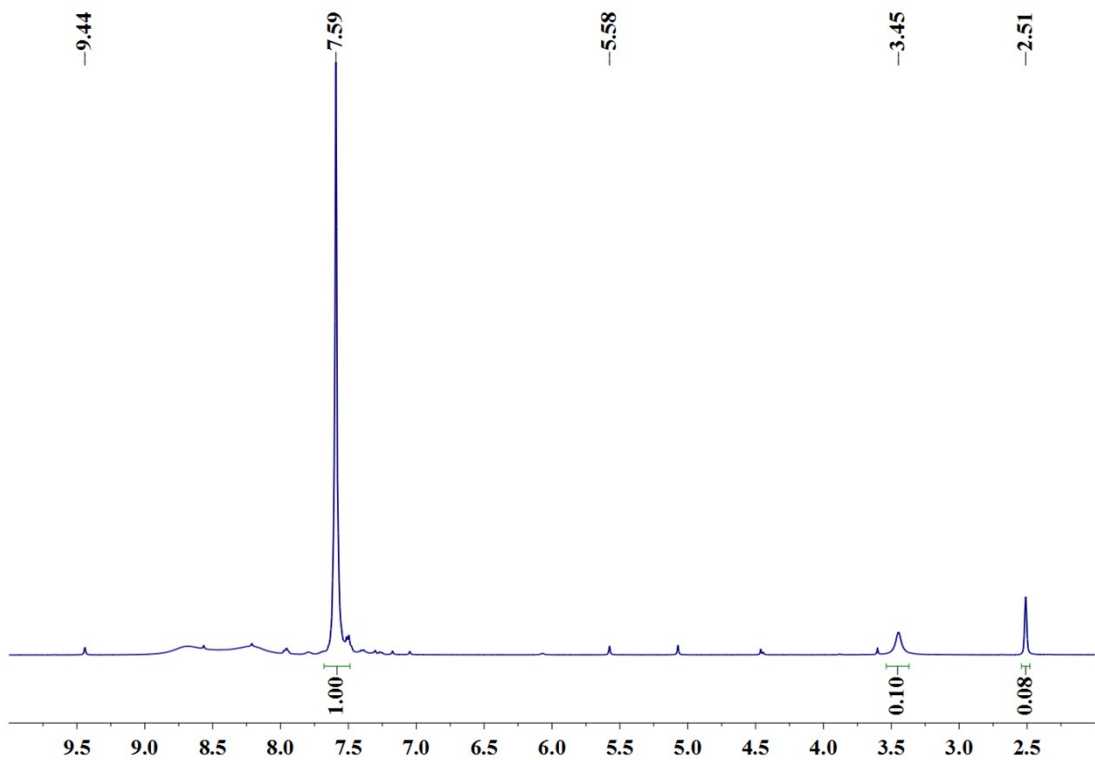


Figure S24. ${}^1\text{H}$ NMR spectrum of 2-(phenylmethylidene)propanedinitrile.

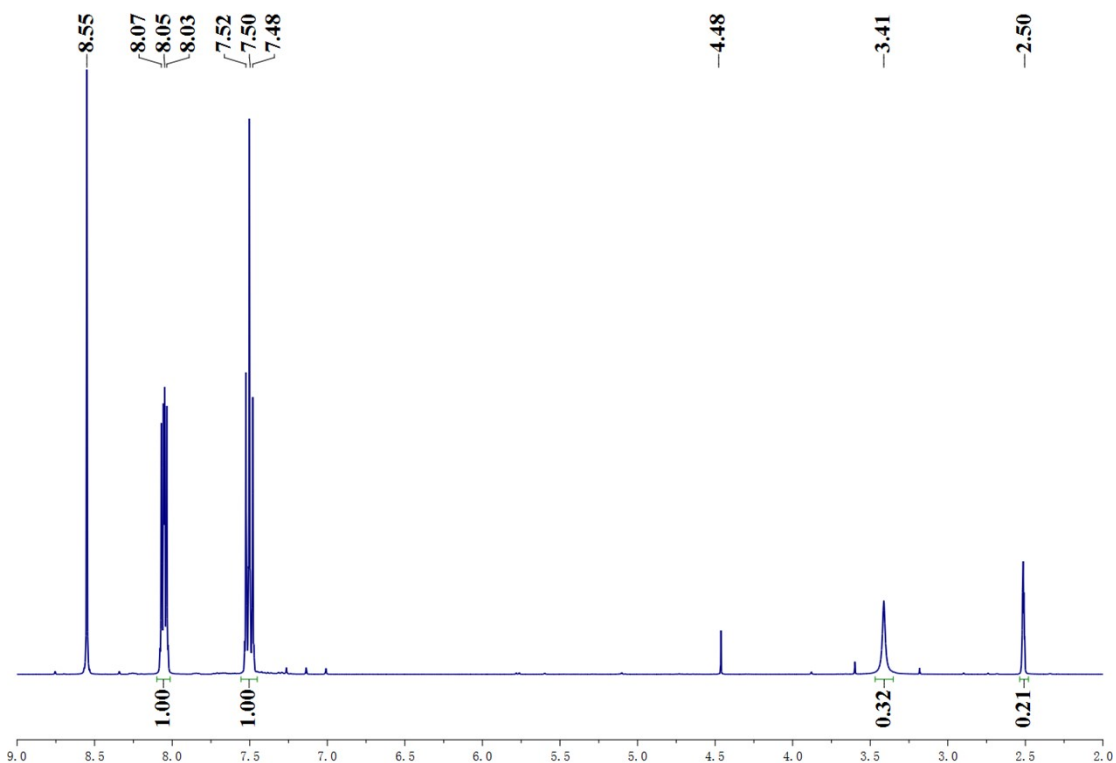


Figure S25. ^1H NMR spectrum of 2-[(4-fluorophenyl)methylidene] propanedinitrile.

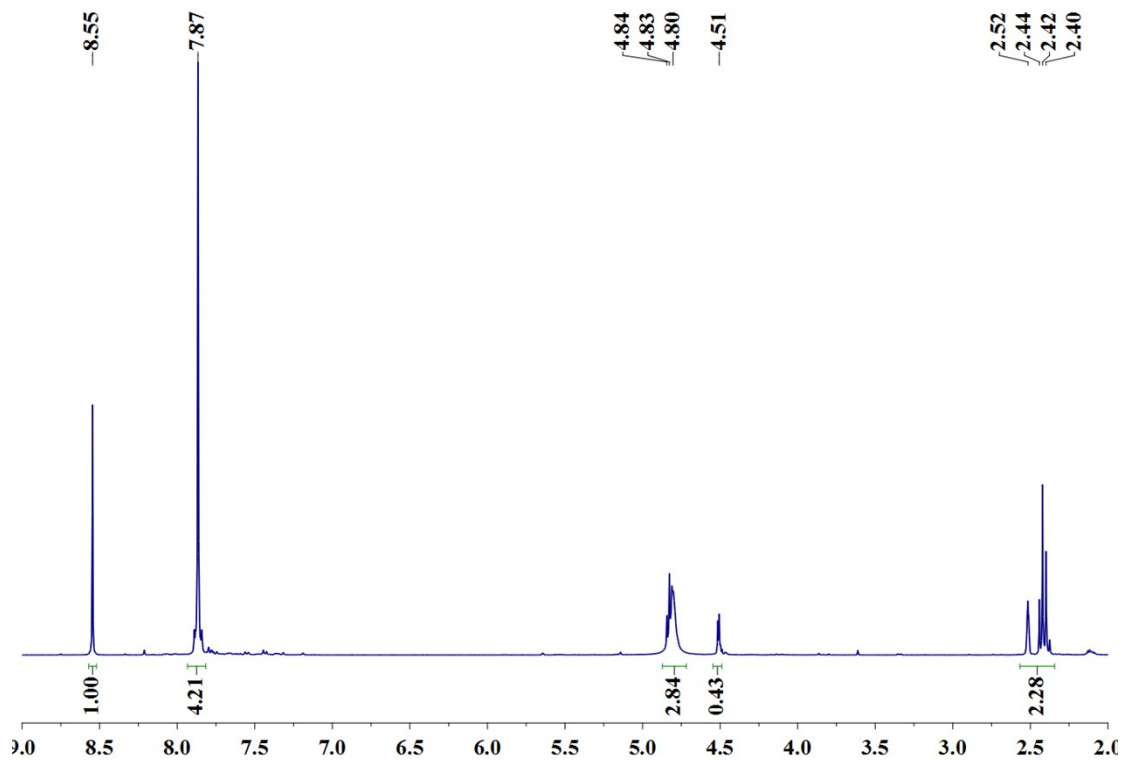


Figure S26. ¹H NMR spectrum of 2-[(4-bromophenyl)methylidene] propanedinitrile.

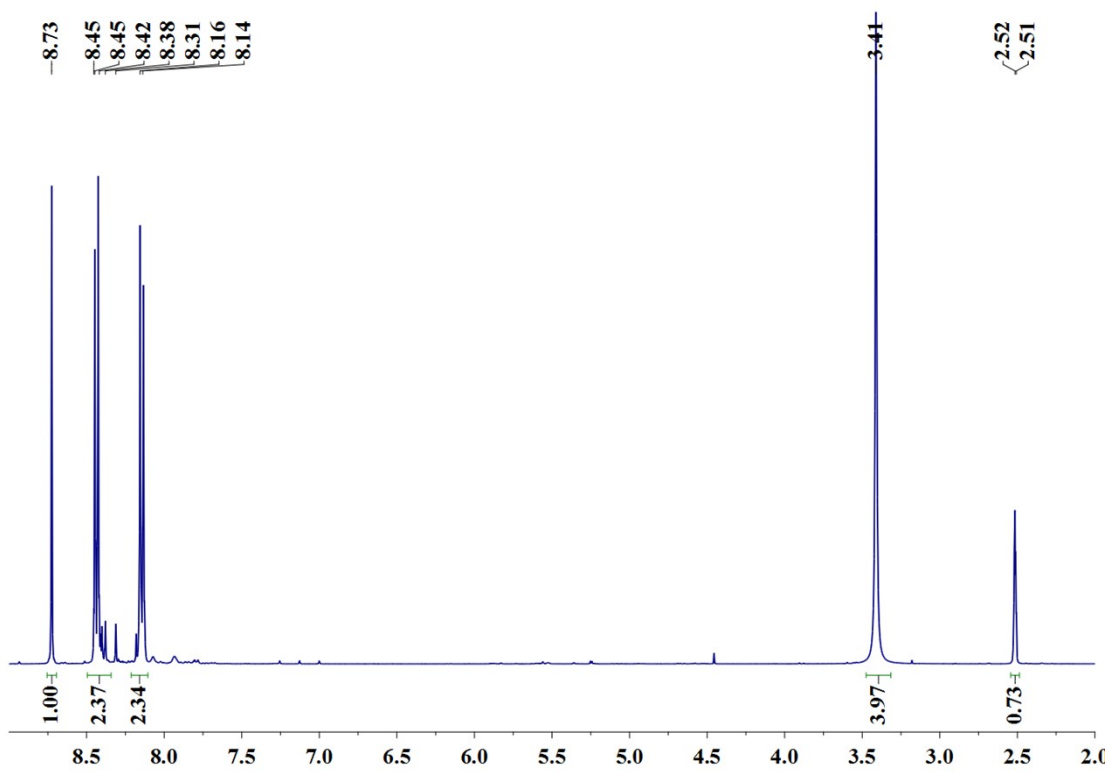


Figure S27. ¹H NMR spectrum of 2-[(4-nitrophenyl) methylidene] propanedinitrile.

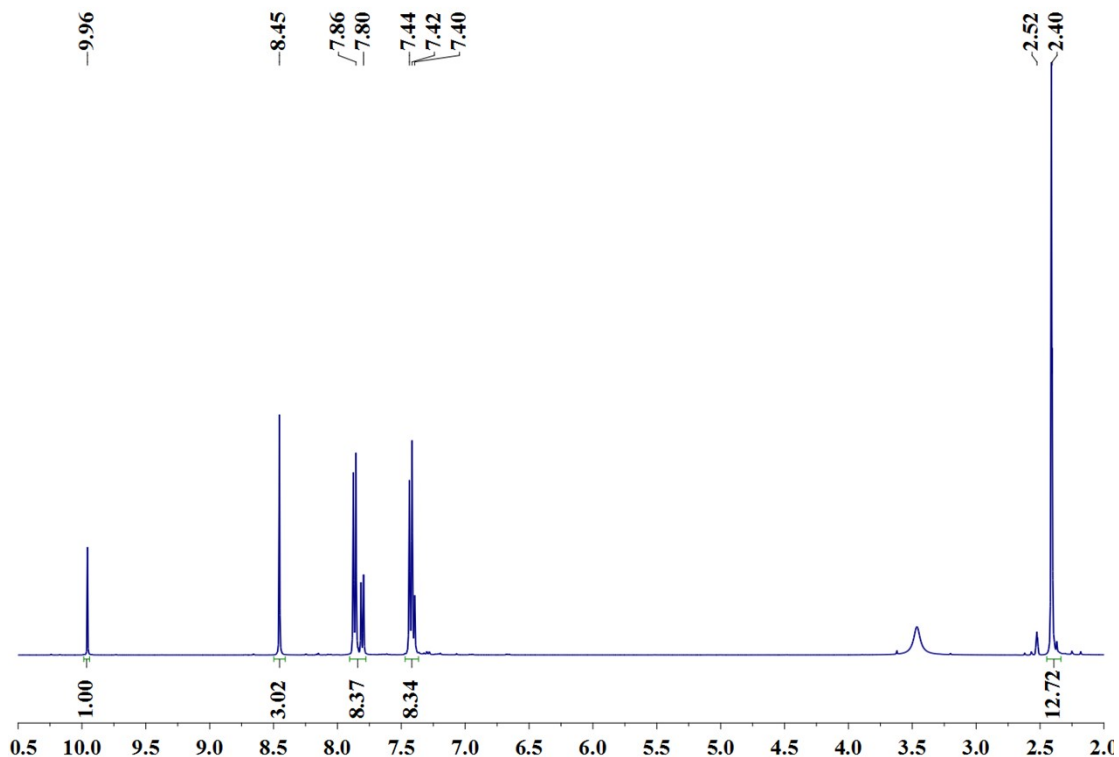


Figure S28. ¹H NMR spectrum of 2-[(4-methylphenyl)methylidene]propanedinitrile.

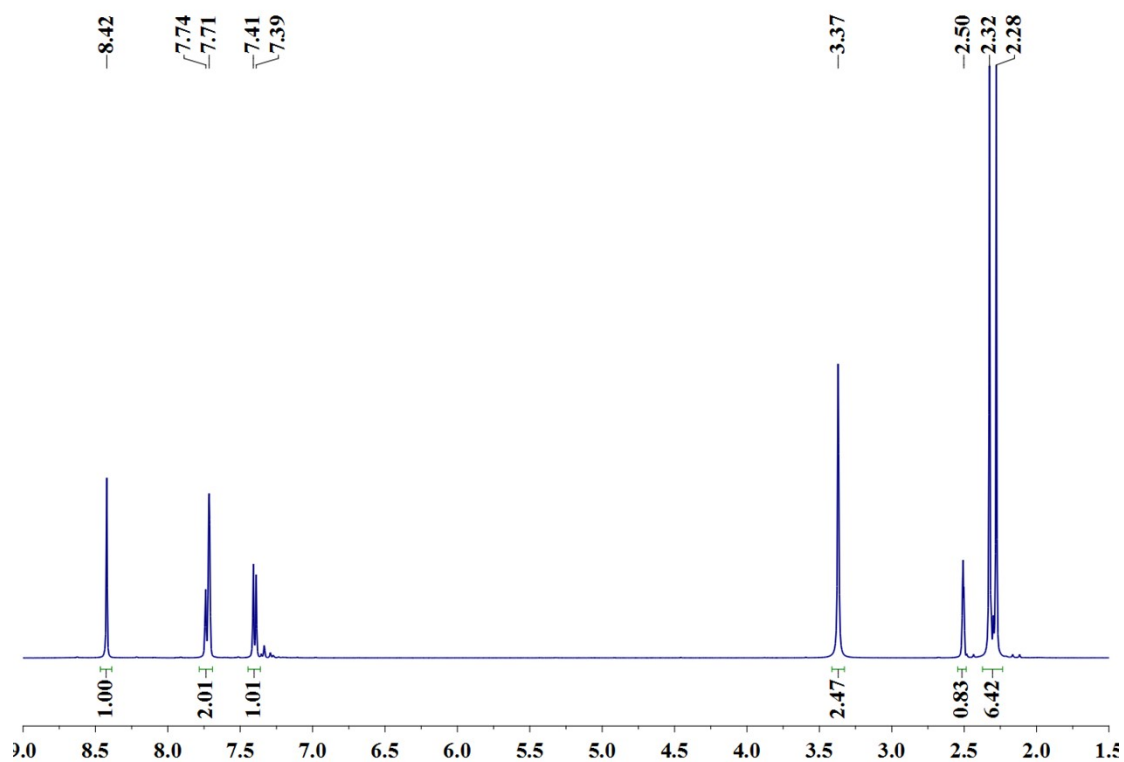


Figure S29. ¹H NMR spectrum of 2-[(3,4-dimethylphenyl)methylidene]propanedinitrile.

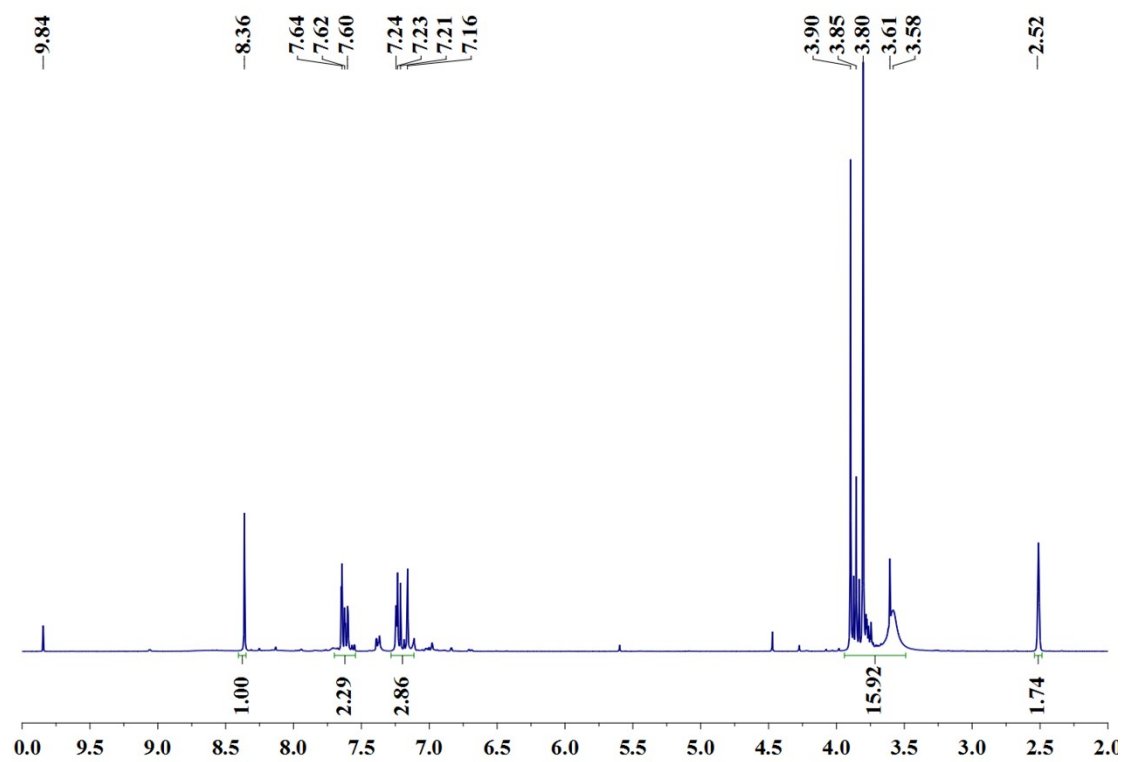


Figure S30. ^1H NMR spectrum of 2-[(3,4-dimethoxyphenyl)methylidene]propanedinitrile.

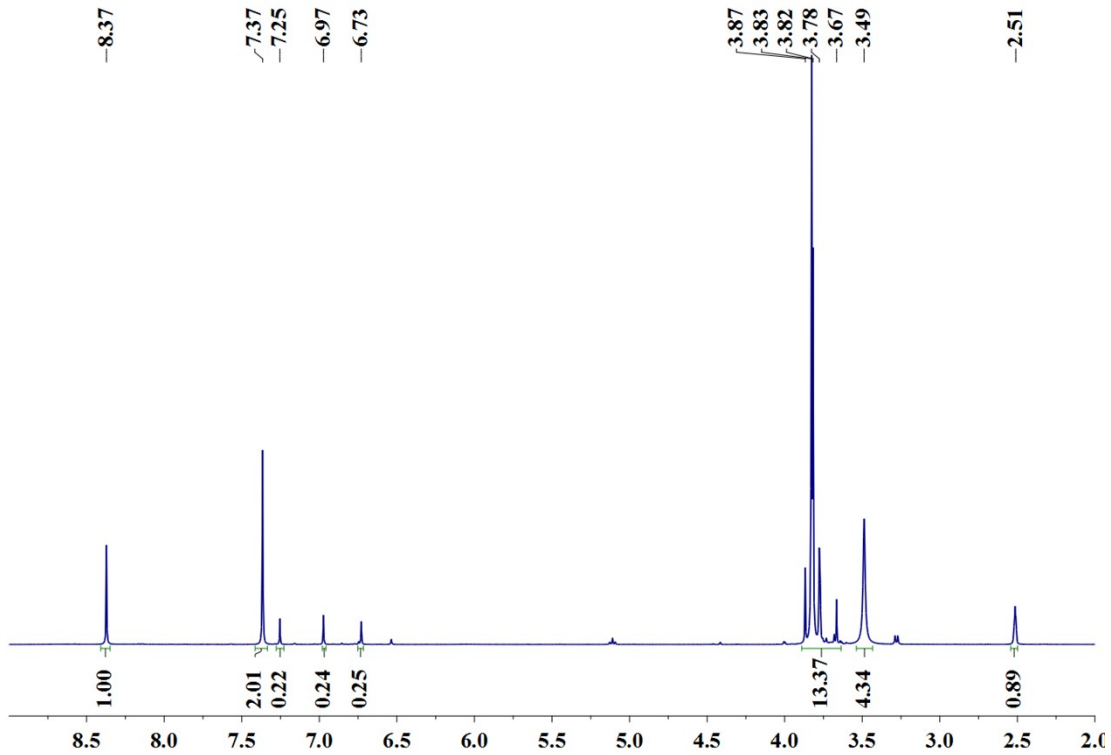


Figure S31. ^1H NMR spectrum of 2-[(3,4,5-trimethoxyphenyl)methylidene]propanedinitrile.

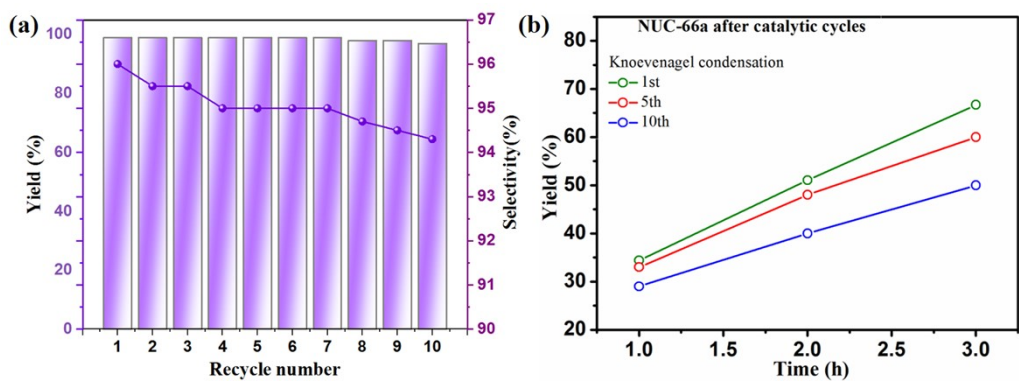


Figure S32. Recyclability study for catalytic activities of **NUC-66a** in Knoevenagel condensation reaction.

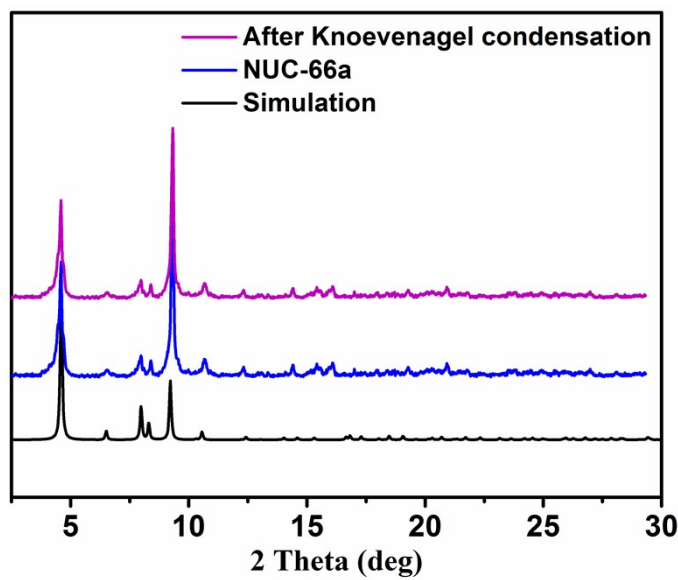


Figure S33. The PXRD patterns of activated and used **NUC-66** after tenth Knoevenagel condensation reactions.

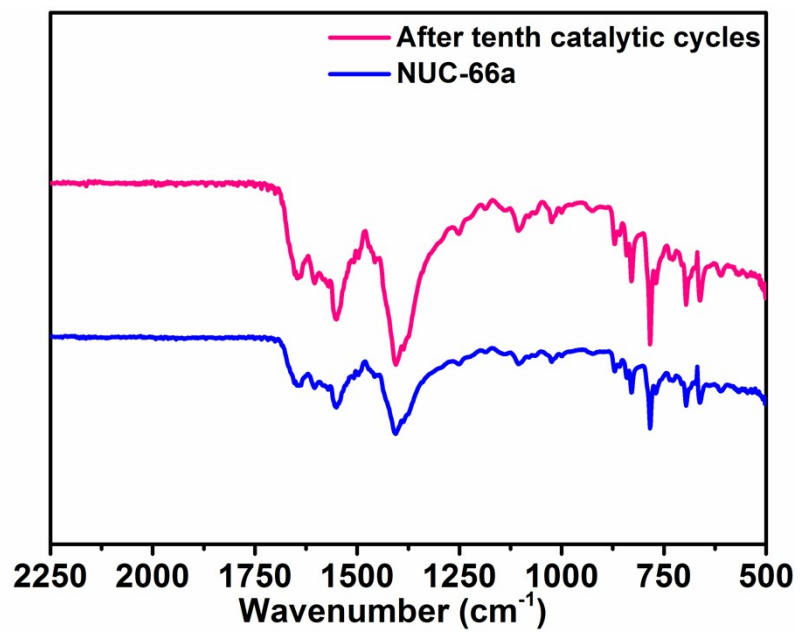


Figure S34. The FT-IR patterns of activated and used **NUC-66** after tenth Knoevenagel condensation reactions.

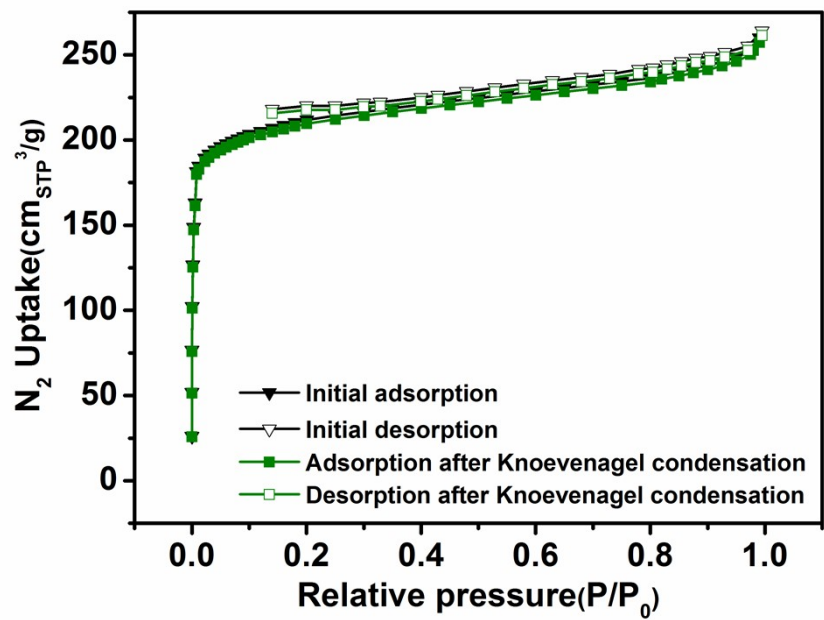


Figure S35. N_2 adsorption isotherms of **NUC-66a** measured after 10 cycles of Knoevenagel condensation reaction, showing negligible change in adsorption amount.

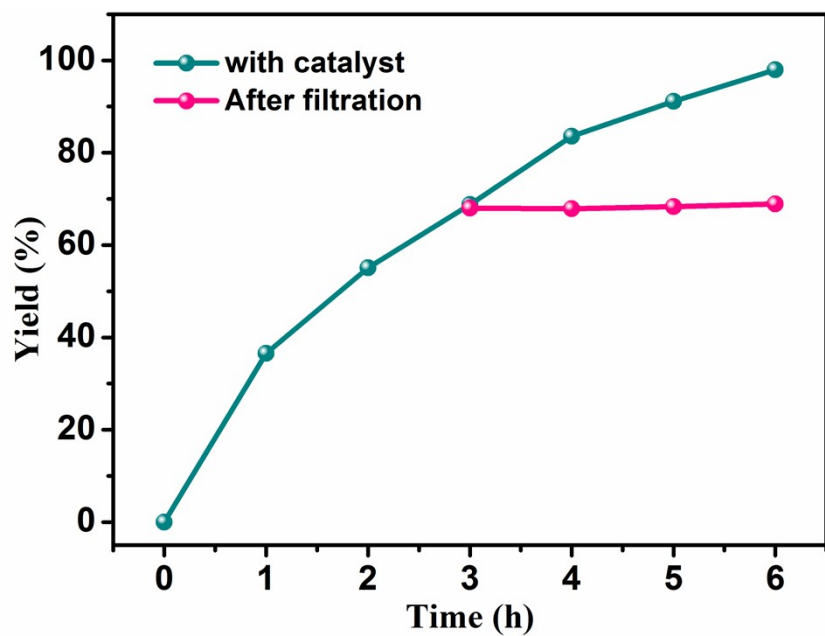


Figure S36. Evidence of heterogeneous nature of NUC-66a in the Knoevenagel condensation reaction.

Reference:

- S1. Gupta, V.; Mandal, S. K. *Inorg. Chem.*, **2022**, *61*, 3086-3096.
- S2. Li, Y.; Zhang, X.; Lan, J.; Li, D.; Wang, Z.; Xu, P.; Sun, J. *ACS Sustainable Chem. Eng.*, **2021**, *9*, 2795–2803.
- S3. Gao, A.; Li, F.; Xu, Z.; Ji, C.; Gu, J.; Zhou, Y. H. *Dalton Trans.*, **2022**, *51*, 2567-2576.
- S4. Wang, W. M.; Wang, W. T.; Wang, M. Y.; Gu, A. L.; Wu, Z. L. *Inorg. Chem.*, **2021**, *60*, 9121-9133.
- S5. Zhu, Y.; Gu, J.; Yu, X.; Zhang, B.; Li, G.; Li, J.; Liu, Y. *Inorg. Chem. Front.*, **2021**, *8*, 4990-4997.
- S6. Yuan, R.; Chen, H.; Zhu, Q. Q.; He, H. *J. Solid State Chem.*, **2021**, *297*, 122036-122042.
- S7. Gao, Z.; Liang, L.; Zhang, X.; Xu, P.; Sun, J. *ACS Appl. Mater. Interfaces*, **2021**, *13*, 61334–61345.
- S8. Parmar, B.; Bisht, K. K.; Rachuri, Y.; Suresh, E. *Inorg. Chem. Front.*, **2020**, *7*, 1082-1107.
- S9. Patel, U.; Patel, P.; Parmar, B.; Dadhania, A.; Suresh, E. *Cryst. Growth Des.*, **2021**, *21*, 1833-1842.
- S10. Yang, W.; Li, H.; Wu, Q.; Ren, Y.; Shi, D.; Zhao, Y.; Jiao, Q. *ACS Sustain. Chem. Eng.*, **2020**, *8*, 18126-18137.
- S11. Wypych, G. *Handbook of Solvents*; Canada, **2014**, 448–454. DOI: 10.1016/c2013-0-13246-1.
- S12. Cai, K.; Tan, W.; Zhao, N.; He, H. *Cryst. Growth Des.*, **2020**, *20*, 4845-4851.
- S13. Qiao, J.; Zhang, B.; Yu, X.; Zou, X.; Liu, X.; Zhang, L.; Liu, Y. *Inorg. Chem.*, **2022**, *61*, 3708-3715.
- S14. Markad, D.; Khullar, S.; Mandal, S. K. *ACS Appl. Nano Mater.*, **2018**, *1*, 5226-5236.
- S15. Chen, H.; Fan, L.; Hu, T.; Zhang, X. *Inorg. Chem.* **2021**, *60*, 7276–7283.
- S16. Qiao, J.; Zhang, B.; Yu, X.; Zou, X.; Liu, X.; Zhang, L.; Liu, Y. *Inorg. Chem.*, **2022**, *61*, 3708–3715.
- S17. Jiang, W.; Yang, J.; Liu, Y. Y.; Song, S. Y.; Ma, J. F. *Inorg. Chem.*, **2017**, *56*, 3036-3043.
- S18. Yao, C.; Zhou, S.; Kang, X.; Zhao, Y.; Yan, R.; Zhang, Y.; Wen, L. *Inorg. Chem.*, **2018**, *57*, 11157-11164.
- S19. Deng, J.-B.; Wang, X.; Ni, Z.-Q.; Zhu, F. *Arab. J. Chem.*, **2020**, *13*, 7482-7489.
- S20. Chen, H.; Fan, L.; Hu, T.; Zhang, X. *Inorg. Chem.* **2021**, *60*, 5005–5013.
- S21. Wang, X. M.; Fan, R. Q.; Qiang, L. S.; Wang, P.; Wang, Y. L. *Dalton Trans.*, **2014**, *43*, 16152-16155.
- S22. Wang, S.; Li, S.; Feng, H.; Yang, W.; Feng, Y. S. *ACS Appl. Mater. Inter.*, **2023**, DOI: 10.1021/acsami.2c22686.
- S23. Lv, Y.; Wang, X.; Jian, C.; Yue, L.; Lin, S.; Zhang, T.; He, Y. *ACS Appl. Nano Mater.*, **2022**, *5*, 18654-18663.
- S24. Liu, X.; Liu, B.; Eubank, J. F.; Liu, Y. *Mater. Chem. Front.*, **2020**, *4*, 182–188.
- S25. Chen, Y.; Zhang, X.; Chen, H.; Drout, R. J.; Chen, Z.; Mian, M. R.; Maldonado, R. R.; Ma, K.; Wang, X.; Xia, Q.; Li, Z.; Islamoglu, T.; Snurr, R. Q.; Farha, O. K. *ACS Appl. Mater. Interfaces*, **2020**, *12*, 44762–44768.
- S26. Fan, W.; Wang, X.; Xu, B.; Wang, Y.; Liu, D.; Zhang, M.; Shang, Y.; Dai, F.; Zhang, L.; Sun, D. *J. Mater. Chem. A*, **2018**, *6*, 24486–24495.